



## Research paper

Glutathione-mediated activation of a disulfide containing Fe<sup>3+</sup> complex

Audrey G. Fikes, Kanchan Aggarwal, Emily L. Que\*

Department of Chemistry, The University of Texas at Austin, 105 E. 24th Street Stop A5300, Austin, TX 78712, United States



## ARTICLE INFO

## Keywords:

Fe<sup>3+</sup> complex  
Caged metal complex  
Disulfide  
Glutathione  
Fenton chemistry  
ROS production

## ABSTRACT

Metal complexes containing ligands that can be cleaved using biological reductants are possible alternatives to traditional photocaged metal ions. This strategy has been demonstrated in this proof-of-concept study with a disulfide containing Fe<sup>3+</sup> complex, **FeL1Cl**. The loss of tight Fe<sup>3+</sup> complexation due to disulfide reduction is observed through a decrease in a ligand to metal charge transfer band in its UV–vis spectrum. The mechanism of this reaction was investigated using mass spectrometry and stopped flow kinetics. A coumarin fluorescence assay was used to determine the ability of this complex to catalyze Fenton chemistry and produce hydroxyl radical. Hydroxyl radical production by **FeL1Cl** was low but in the presence of the reductant glutathione, hydroxyl radical production is increased, suggesting that reduction of the disulfide bond by glutathione uncages the reactivity of the Fe center in this complex.

## 1. Introduction

Caged metal ions are useful tools for studying cellular metal ion homeostasis and have been used to investigate a range of metals including Ca<sup>2+</sup>, Zn<sup>2+</sup>, Fe<sup>2+/3+</sup>, and Cu<sup>2+</sup> [1–7]. Complexes designed for controlled intracellular release of metal ions have historically taken advantage of photolabile ligands that attenuate metal ion binding affinity upon irradiation [4,5]. Two common strategies include photo-induced decrease in ligand donor atom strength [1,3,6,8] and photo-induced ligand cleavage resulting in a decrease in the chelate effect [9–11]. Photocaged metals have been used successfully to probe the role of Ca<sup>2+</sup>, including its role in neurotransmitter release [12], vascular dilation and constriction by astrocytes [13], and glutamate release in astrocytes [14]. However, there are limitations to relying on light as the needed stimulus for uncaging metal ions, including low quantum yields [2,3,7], slow rate of release [2], small changes in metal ion binding affinity [3,15], and often the need to use UV light, which can damage and kill cells. In regard to Fe<sup>3+</sup>, a few photocaged complexes have been reported. Naturally occurring photoactive Fe<sup>3+</sup> siderophore complexes have been investigated [16,17] and have inspired the creation of a siderophore-based trinuclear Fe<sup>3+</sup> complex, which releases Fe<sup>2+</sup> upon irradiation [18]. The photocage FerriCast has also been used to successfully modulate ligand binding affinity for Fe<sup>3+</sup> after UV irradiation [6].

An alternative strategy is the inclusion of a labile bond within the

ligand backbone that can be cleaved *via* methods other than irradiation. Disulfide bonds are an attractive option and have been used extensively as redox controlled triggers for intracellular cargo release [19,20]. Disulfides are easily reduced to thiols, especially in a cellular environment due largely to the high concentrations of glutathione (GSH) which is present at mM levels in the cell [20]. In concurrence with negligible levels of GSH outside the cell, it is easy to envision a disulfide-containing caged metal complex that will be selectively reduced inside a cell and increase the lability of the metal ion due to the subsequent decrease in binding affinity through the chelate effect.

Several disulfide containing metal complexes have been made over the past 40 years [21]. Most transition metal containing disulfide complexes have been characterized primarily using X-ray crystallography [22–25] and have not been investigated for their reactivity with biological reductants. Previously reported complexes have also been synthesized as potential catalysts [26–29] while others have been made to investigate the interactions between thiols, disulfides, and biologically relevant metal ions due to their importance in cellular environments [30,31]. However, the use of disulfide metal complexes as caged metal ions for controlling metal ion reactivity and lability has not been explored. To this end, we have investigated a disulfide containing Fe<sup>3+</sup> complex, **FeL1Cl**, for its reactivity and its possible use for selective de-caging of Fe<sup>3+</sup> in the presence of high concentrations of GSH (Scheme 1).

*Abbreviations:* GSH, glutathione; LMCT, ligand to metal charge transfer; DMSO, dimethyl sulfoxide; MeOH, methanol; DTT, dithiothreitol; HRMS, high resolution mass spectrometry; 7-HC, 7-hydroxycoumarin

\* Corresponding author.

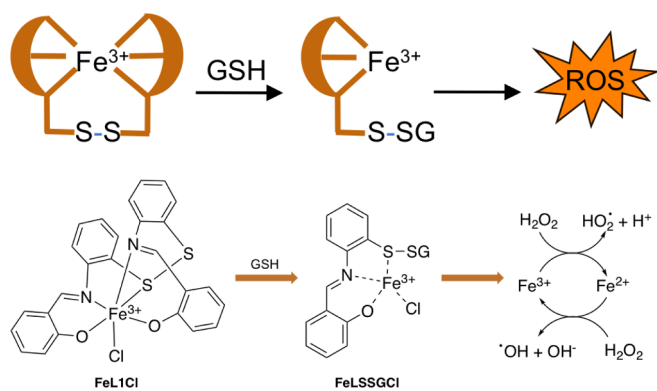
E-mail address: [emilyque@cm.utexas.edu](mailto:emilyque@cm.utexas.edu) (E.L. Que).

<https://doi.org/10.1016/j.ica.2019.03.006>

Received 23 January 2019; Received in revised form 4 March 2019; Accepted 4 March 2019

Available online 05 March 2019

0020-1693/ © 2019 Elsevier B.V. All rights reserved.



Scheme 1. GSH activation of a disulfide containing  $\text{Fe}^{3+}$  complex.

## 2. Results

The disulfide containing complex **FeL1Cl** was synthesized as reported in literature [24]. The ligand was synthesized *via* condensation of 2,2'-diaminodiphenyl disulfide with salicylaldehyde. The absorbance spectrum of the complex is characterized by an intense phenolato to  $\text{Fe}^{3+}$  ligand to metal charge transfer (LMCT) band around 546 nm ( $\epsilon = 3900 \text{ M}^{-1} \text{ cm}^{-1}$ ) in DMSO [27] and 562 nm ( $\epsilon = 2860 \text{ M}^{-1} \text{ cm}^{-1}$ ) in  $\text{CH}_2\text{Cl}_2$  [32]. The magnetic moment was determined to be  $6.2 \mu_B$  indicating a high spin  $\text{Fe}^{3+}$  complex. The ligand has an irreversible reduction at  $-1.91 \text{ V}$  corresponding to the imine while the disulfide redox couple has an  $E_{1/2} = -1.26 \text{ V}$  (Fig. S1A) which is typical of aromatic disulfides [33]. The complex has an  $\text{Fe}^{3+}/\text{Fe}^{2+}$  redox couple at  $-1.48 \text{ V}$ . The reduction potential for the imine is shifted to  $-0.721 \text{ V}$  while the  $E_{1/2}$  for the disulfide is shifted to  $-0.575 \text{ V}$  (Fig. S1B). The positive shift in the reduction potential of both the imine and disulfide are indicative of coordination of the nitrogen and sulfur, respectively, to the  $\text{Fe}^{3+}$ . The resulting polarization of the bonds makes both moieties easier to reduce as indicated by the change in reduction potentials.

To determine the feasibility of GSH mediated  $\text{Fe}^{3+}$  release from the initial **FeL1Cl** complex *via* disulfide reduction, absorbance of the LMCT was monitored upon addition of GSH. As expected, a decrease in the LMCT is seen with GSH addition, indicating decomplexation of  $\text{Fe}^{3+}$  (Fig. 1A, Fig. S2). A similar decrease in the LMCT is also seen upon addition of other reductants, including DTT and sodium dithionite (Fig. S3). These observed changes differ from those of the reaction of ligand L1 with GSH (Fig. 1B), in which changes are only observed below 450 nm. This suggests that the decrease in LMCT is a result of a change in the coordination of the metal center, likely due to loss of phenolato- $\text{Fe}^{3+}$  coordination bonds. The products of the reduction were evaluated using high resolution mass spectrometry (HRMS) (Table S1). Two species containing GSH adducts were detected indicating that loss of  $\text{Fe}^{3+}$  coordination is due to cleavage of the ligand disulfide by GSH (Figs. S11 and S12). Importantly, no **FeL1Cl** is detected by HRMS in the

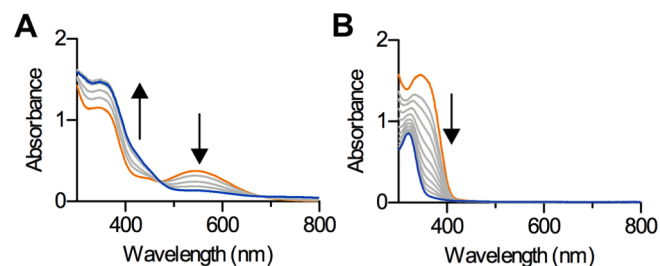


Fig. 1. UV-vis spectra of (A)  $100 \mu\text{M}$  **FeL1Cl** in DMSO after addition of 1 equiv. of GSH and (B)  $100 \mu\text{M}$  L1 in DMSO after addition of 10 equiv. of GSH. A decrease in the LMCT band at 546 nm for **FeL1Cl**, which is not seen for L1, indicates loss tightly bound  $\text{Fe}^{3+}$ .

presence of GSH, suggesting that  $\text{Fe}^{3+}$  is no longer bound to the parent complex. We note that in the absence of GSH, **FeL1Cl** is readily detected under the same HRMS conditions. The free ligand, L1, is detected both before (Figs. S13 and S14) and after addition of GSH to **FeL1Cl** (Figs. S15 and S16). Detection of L1 in the control solution containing only **FeL1Cl** is likely due to loss of  $\text{Fe}^{3+}$  during the ionization process. After addition of GSH, since no intact **FeL1Cl** is detected, detection of L1 is assumed to be due to continued disulfide exchange leading to the reformation of L1 without any  $\text{Fe}^{3+}$  bound. This is supported by the observation that there is no reappearance of the LMCT and the corresponding deep purple color, indicating that  $\text{Fe}^{3+}$  is no longer tightly bound to the ligand.

The kinetics of the disulfide cleavage were also investigated. The reaction was predicted to be first order in both reactants and second order overall, as shown in Eq. (1). Under *pseudo* first order conditions with excess GSH, the rate law was expected to become Eq. (2).

$$r = k[\text{GSH}][\text{FeL1Cl}] \quad (1)$$

$$r = k_{\text{obs}}[\text{FeL1Cl}] \quad (2)$$

The data shows, however, that in the presence of excess GSH, the reaction is second order in **FeL1Cl** (Fig. 2B). This can be explained through the proposed mechanism in Eqs. (3) and (4) and Fig. 2D. Initial disulfide cleavage by GSH results in the creation of a free thiol, LSH, from the complex. This free thiol is available to reduce intact complexes of **FeL1Cl**. Because of this, the observed rate law is second order in **FeL1Cl** and first order in GSH (Eq. (5)). When carried out with excess GSH, the rate law is simplified to Eq. (6).



$$r \approx k[\text{GSH}][\text{FeL1Cl}]^2 \quad (5)$$

$$r \approx k_{\text{obs}}[\text{FeL1Cl}]^2 \quad (6)$$

As expected, the reaction between **FeL1Cl** and GSH was first order in GSH over a wide range of GSH concentrations as shown by the plot of  $k_{\text{obs}}$  vs the initial GSH concentration (Fig. S5C). Unexpectedly, a plot of  $k_{\text{obs}}$  vs initial **FeL1Cl** concentration shows that  $k_{\text{obs}}$  decreases with increasing **FeL1Cl** concentration in a linear fashion as opposed to increasing in a quadratic manner (Fig. 2C). This is most likely due to interference in absorbance caused by complexes of weakly bound  $\text{Fe}^{3+}$  with the resulting products from the reaction. This includes an  $\text{Fe}^{3+}$  complex formed with a ligand-GSH adduct, **FeLSSGCl** (Fig. 2D), which is observed by HRMS after the reaction of **FeL1Cl** with GSH (Fig. S19) and another  $\text{Fe}^{3+}$  complex that forms with two intact L1 ligands, observed in small amounts *via* HRMS both before and after reduction with GSH (Table S1, Figs. S17 and S18). Mild interference in absorbance between 500 and 600 nm can also be caused by complexation of  $\text{Fe}^{3+}$  with GSH itself [34]. When we modeled this proposed mechanism (KinTek Explorer software [35]) including absorbance interference and considering Eq. (3) as faster than Eq. (4), the same trend is seen in that the  $k_{\text{obs}}$  decreases linearly with increasing **FeL1Cl** concentration (Fig. S6B).

In order to demonstrate that the intact **FeL1Cl** complex fully sequesters  $\text{Fe}^{3+}$ , the complex's ability to catalyze Fenton chemistry was investigated. Hydroxyl radicals react with coumarin to produce 7-hydroxycoumarin (7-HC), which fluoresces at 400 nm [36–38]. This reaction with coumarin takes place readily in the presence of labile  $\text{Fe}^{3+}$  and  $\text{H}_2\text{O}_2$ . Comparison of the relative integrated fluorescence of 7-HC formed under different reaction conditions can demonstrate the ability of **FeL1Cl** to produce ROS only after reaction with GSH. The ability of  $\text{FeCl}_3$  and **FeL1Cl** to catalyze hydroxyl radical formation in the presence and absence of GSH was compared (Fig. 3).  $\text{FeCl}_3$  alone leads to high levels of 7-HC fluorescence, which are not significantly affected by the presence of equimolar GSH or L1, as mixture of  $\text{FeCl}_3$  and L1 at room temperature does not lead to the formation of **FeL1Cl**. When

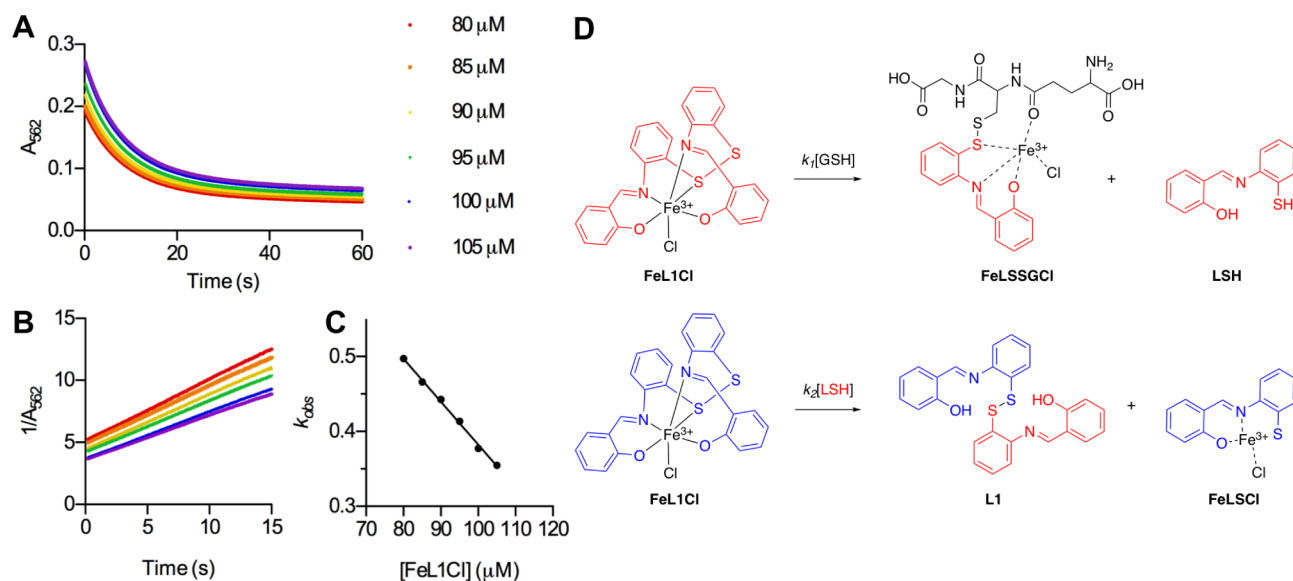


**Fig. 2.** (A) The change in absorbance at 562 nm over time for the reaction of **FeL1Cl** (80–105  $\mu$ M) with 1 mM GSH in MeOH. (B) A plot of  $1/A_{562nm}$  vs time for the initial 15 s of the reaction between constant GSH and varying **FeL1Cl** concentrations; the linear relationship demonstrates that the reaction is second order in **FeL1Cl**. The slopes of the lines give the  $k_{obs}$  values. (C) A decrease in  $k_{obs}$  values with increasing [**FeL1Cl**] is observed, indicating interference at the observed wavelength (562 nm) due to products from the reaction. As the concentration of **FeL1Cl** increases, the concentration of interfering products increases leading to the unexpected relationship between  $k_{obs}$  and [**FeL1Cl**]. (D) Proposed mechanism that explains the decreasing trend in  $k_{obs}$  and the second order dependence on **FeL1Cl**. The first step involves the reaction of **FeL1Cl** with GSH leading to the formation of FeLSSGCl, which is proposed to be one of the possible species absorbing weakly at 562 nm and causing interference. In step two, the free thiol LSH, from step one, reacts rapidly with remaining **FeL1Cl** leading to an overall reaction mechanism that appears to be second order in **FeL1Cl**.

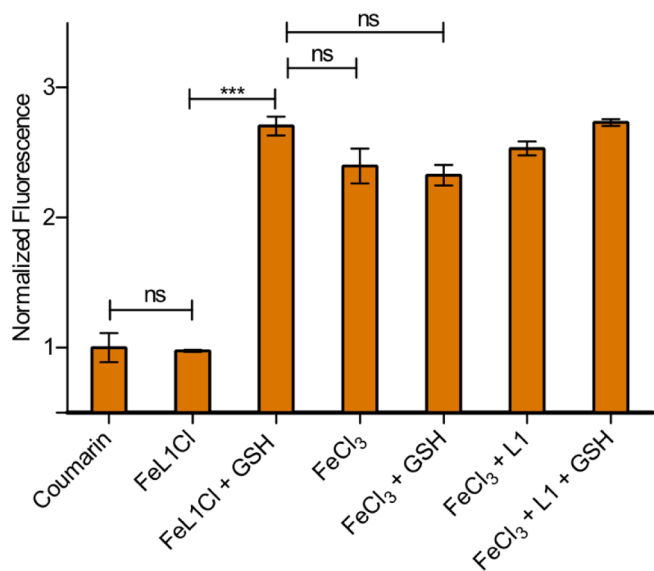


**Fig. 3.** Normalized fluorescence of 7-hydroxycoumarin produced from the reaction of coumarin with hydroxyl radical in the presence of  $H_2O_2$ . No difference in fluorescence signal is observed between the control containing only coumarin and the sample with **FeL1Cl**, indicating that the  $Fe^{3+}$  is effectively caged. In the presence of GSH, the fluorescence signal increases due to the uncaging of the  $Fe^{3+}$  which is then free to catalyze hydroxyl radical production. Fluorescence levels observed after addition of GSH to **FeL1Cl** are similar to those produced by  $FeCl_3$ . Data represents mean values ( $n = 3$ )  $\pm$  the standard deviation (\*\*\*)  $p < 0.0001$ .

**FeL1Cl**,  $H_2O_2$ , and coumarin were combined, similar levels of fluorescence were observed as in the control reaction between coumarin and  $H_2O_2$  in the absence of any  $Fe^{3+}$  source. These results indicate that the complex is unable to catalyze hydroxyl radical formation due to its fully occupied coordination sphere. Upon incubation of **FeL1Cl** with GSH, the fluorescence levels increased, suggesting that cleavage of the

disulfide bond by GSH uncages the  $Fe^{3+}$  reactivity and restores its ability to catalyze formation of ROS in the presence of  $H_2O_2$ . These results demonstrate this proof of concept study that disulfide containing ligands can be used to make caged metal complexes that effectively mask a metal ion's reactivity until exposure to a reducing environment uncages the metal, thus restoring reactivity.

### 3. Conclusions

In conclusion, a disulfide-containing  $Fe^{3+}$  complex has been studied as an alternative to photocaged metals for controlling  $Fe^{3+}$  reactivity through ligand centered reduction. This proof-of-concept study demonstrates the feasibility of disulfide dependent caged metal complexes that circumvents common problems associated with photolabile ligands. Current efforts are geared towards the development of aqueous-compatible complexes for biological studies of the interplay of metal ion homeostasis and oxidative stress.

### 4. Experimental

#### 4.1. Materials

All chemicals and solvents were purchased from Alfa Aesar and Fisher Scientific and used as received.  $^1H$  and  $^{13}C$  NMR spectrum were acquired on a 400 MHz Agilent MR spectrometer. NMR samples were prepared in  $DMSO-d_6$  and chemical shifts are reported in ppm. Electrospray Ionization Mass Spectrometry (ESI-MS) was performed by the Mass Spectrometry Facility of the Department of Chemistry at UT Austin. UV–vis spectroscopic studies were performed using an Agilent Cary 60 UV–vis Spectrophotometer. Kinetic measurements were made using a Hi-Tech Scientific SFA-20 Rapid Kinetics Accessory in tandem with an Agilent 8453 UV–vis Spectrophotometer. Cyclic voltammetry was carried out using a CHI 660D electrochemical workstation from the UT Austin Center for Electrochemistry. Fluorescence measurements were made using an Agilent Cary Eclipse Fluorescence Spectrophotometer.

#### 4.2. Synthesis of FeL1Cl [24,32]

2,2'-Diaminodiphenyl disulfide (500.4 mg, 2.015 mmol) was dissolved in 12 mL MeOH. Salicylaldehyde (0.211 mL, 2.015 mmol) was dissolved in 1.5 mL MeOH and added to the first solution. Lithium (14.0 mg, 2.017 mmol) was dissolved in 5 mL MeOH and added to the ligand solution and stirred at room temperature. A 3 mL MeOH solution of FeCl<sub>3</sub> (163.4 mg, 1.007 mmol) was added dropwise to the solution. The solution was refluxed for 30 min and allowed to cool to room temperature. A dark solid precipitated out of solution. Filtering and washing with hot MeOH gave pure product with a yield of 61%. Product formation was confirmed through UV-vis spectroscopy and HRMS.  $\epsilon_{562\text{nm}}$  in DCM: 2860 M<sup>-1</sup> cm<sup>-1</sup> [32]. HR ESI-MS (ESI<sup>+</sup>, MeOH): calculated for [M-Cl]<sup>+</sup> 510.0154, found 510.0155.

#### 4.3. Synthesis of L1 [28]

A modified literature procedure was used to synthesize L1 [28]. 2,2'-diaminodiphenyl disulfide (439.6 mg, 1.770 mmol) and salicylaldehyde (0.463 mL, 4.421 mmol) were combined in 60 mL EtOH. A yellow solid immediately began precipitating. The mixture was stirred for 15 min at room temperature. The mixture was refrigerated for three hours and then filtered and washed with cold EtOH to give a yield of 90%. <sup>1</sup>H NMR (400 MHz, DMSO-*d*<sub>6</sub>)  $\delta$  12.56 (s, 1H), 9.02 (s, 1H), 7.71 (dd, *J* = 7.7, 1.8 Hz, 1H), 7.56 (dd, *J* = 7.9, 1.5 Hz, 1H), 7.50 (dd, *J* = 7.9, 1.4 Hz, 1H), 7.46 (ddd, *J* = 8.1, 7.3, 1.7 Hz, 1H), 7.36 (td, *J* = 7.6, 1.5 Hz, 1H), 7.29 (td, *J* = 7.6, 1.4 Hz, 1H), 7.04–6.97 (m, 2H). <sup>13</sup>C NMR (DMSO-*d*<sub>6</sub>, 400 MHz):  $\delta$  164.1, 160.6, 146.5, 134.4, 133.2, 130.8, 128.6, 128.4, 126.6, 119.9, 119.0, 117.2. LR ESI-MS (ESI<sup>+</sup>, MeOH): calculated for [M+H]<sup>+</sup> 457.1, found 457.1.

#### 4.4. UV-vis spectroscopy

To study the reaction of FeL1Cl with different reductants, the change in the UV-vis spectrum of 100  $\mu$ M FeL1Cl was monitored while GSH, DTT, and sodium dithionite were titrated into the solution, respectively. The studies were carried out in DMSO and MeOH. Data was collected with an Agilent Technologies Cary 60 UV-vis spectrometer. Stock solutions of FeL1Cl (1 mM) were prepared in DMSO or MeOH. GSH stock solution (100 mM) was made using 1:1 water:DMSO. Stock solutions of DTT (100 mM) were made in DMSO or MeOH. Stock solutions of Na<sub>2</sub>S<sub>2</sub>O<sub>4</sub> (100 mM) were made in water. Control studies were done with equivalent amounts of water containing no reductant to demonstrate that changes in the UV-vis spectrum are due to the reaction of FeL1Cl with the reductant and not hydrolysis of FeL1Cl due to the presence of water.

#### 4.5. Cyclic voltammetry

Electrochemical data was collected with a CHI 660D electrochemical workstation. Measurements of a 2 mM solution of FeL1Cl and L1 were recorded at 100 mV/s in a glovebox. A three-electrode cell was used, with a platinum electrode as the working electrode, an Ag/Ag<sup>+</sup> non-aqueous electrode as a reference electrode (a 10 mM solution of AgNO<sub>3</sub> in DMF was used as a Ag<sup>+</sup> source), and a platinum wire auxiliary counter electrode. Bn<sub>4</sub>NBF<sub>4</sub> (0.1 M) was used as the electrolyte and the spectra were calibrated versus ferrocene.

#### 4.6. Mass spectrometry

High resolution ESI-FIA-MS and ESI-LC-MS data was collected on an Agilent Q-TOF LC/MS. Reactions were carried out in methanol with an initial FeL1Cl concentration of 100  $\mu$ M and equimolar amounts of GSH. Samples were analyzed within one hour of GSH addition. Control samples contained only 100  $\mu$ M FeL1Cl and no GSH.

#### 4.7. Kinetics

Kinetic experiments were carried out in MeOH at 26 °C with an excess amount of GSH. FeL1Cl has a strong LMCT at 562 nm, which disappears upon disulfide reduction and concomitant Fe<sup>3+</sup> release. Thus the change in absorbance at 562 nm was monitored over time. Second order dependence on FeL1Cl was determined by holding [GSH] concentration constant (1.0 mM) and varying initial [FeL1Cl] concentration between 80 and 105  $\mu$ M. The pseudo second-order *k*<sub>obs</sub> values were determined by plotting 1/A and obtaining the slopes of the resulting linear plots. A graph of *k*<sub>obs</sub> values vs initial [FeL1Cl] gives a line with a negative slope indicating formation of a product that has weak interfering absorbance around 562 nm (see Kinetics Modeling below.) First order dependence on GSH was determined by keeping [FeL1Cl] constant (100  $\mu$ M) and varying the initial [GSH] from 50  $\mu$ M to 1.4 mM. The *k*<sub>obs</sub> values were obtained by plotting 1/A. A graph of *k*<sub>obs</sub> vs initial [GSH] gives a straight line indicating first order dependence on GSH. The slope of the line gives a third order rate constant of 2.0 M<sup>-2</sup> s<sup>-1</sup>.

#### 4.8. Kinetics modeling with KinTek explorer

The simulations for the possible mechanism for FeL1Cl reduction by GSH were done using KinTek Explorer software [35]. The model used was:



The forward rate for each equation were set so that *k*<sub>1</sub> > *k*<sub>2</sub> and the backward rates were set to small values as both reactions are irreversible. The output was set to:

$$a * \text{FeL1Cl} + b * \text{FeLSSGCl}$$

where a and b are the extinction coefficients for the absorbance of FeL1Cl and FeLSSGCl. They were set in such a way that a was higher than b. The concentrations of GSH and FeL1Cl were kept similar to the experimental conditions. The data generated for total absorbance versus time under the set conditions was fitted to the following exponential equation:

$$Y = Ae^{(-kt)} + B$$

where A is the amplitude, k is the rate constant, and B is a constant. The rate was plotted with respect to concentration of variable species. It should be noted that simulations were run to confirm the proposed mechanism based on the experimental data and not used to calculate the simulated *k*<sub>obs</sub> values, for several reasons. The absolute values of *k*<sub>1</sub> and *k*<sub>2</sub> are unknown as are the extinction coefficients of the interfering species. In addition to this, the kinetics model in the simulations are fixed throughout the time period, while under experimental conditions, it might change with time as the relative concentration of each species varies. For this reason, simulated *k*<sub>obs</sub> values do not necessarily match those obtained experimentally.

#### 4.9. Coumarin hydroxylation fluorescence assay

In order to determine that ability of FeL1Cl to catalyze hydrogen peroxide induced ROS production in the presence and absence of GSH, a coumarin hydroxylation assay was used [38]. Coumarin reacts with hydroxyl radical to yield 7-hydroxycoumarin, which fluoresces around 400 nm in MeOH. Comparison of the integrated fluorescence of reaction solutions containing coumarin, H<sub>2</sub>O<sub>2</sub>, and Fe<sup>3+</sup> indicates the relative amount of hydroxyl radicals produced. Reactions containing FeL1Cl in the absence and presence of GSH were compared to reactions containing FeCl<sub>3</sub> with and without GSH. Control reactions containing L1 and FeCl<sub>3</sub> (both with and without GSH) were also carried out to demonstrate the necessity of the intact FeL1Cl complex to mitigate

hydroxy radical production. Reactions were carried out in degassed MeOH in an anaerobic chamber to prevent quenching of the hydroxyl radical by oxygen. All stock solutions were made in an anaerobic chamber using degassed solvents. Stock solutions of coumarin (5 mM), FeCl<sub>3</sub> (5 mM), FeL1Cl (1 mM), and H<sub>2</sub>O<sub>2</sub> (50 mM) were made MeOH. A 100 mM solution of GSH was made in water. This solution was used to make a 5 mM stock solution of GSH in MeOH. A solution of L1 (12.584 mM) was made in EtOAc. This solution was used to make the final stock solution of L1 (135.14 μM) in MeOH. The final concentrations of coumarin and H<sub>2</sub>O<sub>2</sub> in all the samples were 1 mM each. The final concentrations of either FeCl<sub>3</sub> or FeL1Cl was 100 μM. The final concentration of GSH, when present, was 100 μM. The final concentration of L1, when present, was 100 μM. Fluorescence measurements of the reaction solutions were taken after 16 h of incubation. The excitation wavelength was 344 nm (slit width 20.) Total fluorescence was measured by integrating the fluorescence spectra from 375 nm to 640 nm. All samples were performed in triplicate.

### Acknowledgements

This work was funded by a grant from the Welch Foundation (F-1883) and start-up funds from the University of Texas at Austin. The authors thank Prof. Aimin Liu and Christopher I. Davis from the University of Texas at San Antonio for use of their Hi-Tech Scientific SFA-20 Rapid Kinetics Accessory and Agilent 8453 UV-vis Spectrophotometer for stopped flow kinetic studies. We also acknowledge the use of a Bruker AVIII HD500 with Prodigy liquid nitrogen cryoprobe supported by NIH grant 1 S10OD021508.

### Appendix A. Supplementary data

Supplementary data to this article can be found online at <https://doi.org/10.1016/j.ica.2019.03.006>.

### References

- [1] R.Y. Tsien, R.S. Zucker, Control of cytoplasmic calcium with photolabile tetra-carboxylate 2-nitrobenzhydryl chelators, *Biophys. J.* 50 (5) (1986) 843–853.
- [2] S.R. Adams, J.P.Y. Kao, G. Grynkiwicz, A. Minta, R.Y. Tsien, Biologically useful chelators that release Ca<sup>2+</sup> upon illumination, *J. Am. Chem. Soc.* 110 (10) (1988) 3212–3220.
- [3] C. Gwizdala, D.P. Kennedy, S.C. Burdette, ZinCast-1: a photochemically active chelator for Zn<sup>2+</sup>, *Chem. Commun.* 45 (2009) 6967–6969.
- [4] K.L. Ciesiński, K.J. Franz, Keys for unlocking photolabile metal-containing cages, *Angew. Chem.* 50 (4) (2011) 814–824.
- [5] C. Gwizdala, S.C. Burdette, Following the Ca<sup>2+</sup> roadmap to photocaged complexes for Zn<sup>2+</sup> and beyond, *Curr. Opin. Chem. Biol.* 17 (2) (2013) 137–142.
- [6] D.P. Kennedy, C.D. Incarvito, S.C. Burdette, FerriCast: a macrocyclic photocage for Fe<sup>3+</sup>, *Inorg. Chem.* 49 (3) (2010) 916–923.
- [7] D.P. Kennedy, D.C. Brown, S.C. Burdette, Probing nitrobenzhydryl uncaging mechanisms using FerriCast, *Org. Lett.* 12 (20) (2010) 4486–4489.
- [8] J. Cui, R.A. Gropeanu, D.R. Stevens, J. Rettig, A.D. Campo, New photolabile BAPTA-based Ca<sup>2+</sup> cages with improved photorelease, *J. Am. Chem. Soc.* 134 (18) (2012) 7733–7740.
- [9] J.H. Kaplan, G.C. Ellis-Davies, Photolabile chelators for the rapid photorelease of divalent cations, *Proc. Natl. Acad. Sci. U.S.A.* 85 (17) (1988) 6571–6575.
- [10] H.M.D. Bandara, D.P. Kennedy, E. Akin, C.D. Incarvito, S.C. Burdette, Photoinduced release of Zn<sup>2+</sup> with ZinCleave-1: a nitrobenzyl-based caged complex, *Inorg. Chem.* 48 (17) (2009) 8445–8455.
- [11] K.L. Ciesiński, K.L. Haas, M.G. Dickens, Y.T. Tesema, K.J. Franz, A photolabile ligand for light-activated release of caged copper, *J. Am. Chem. Soc.* 130 (37) (2008) 12246–12247.
- [12] K. Wadel, E. Neher, T. Sakaba, The coupling between synaptic vesicles and Ca<sup>2+</sup> channels determines fast neurotransmitter release, *Neuron* 53 (4) (2007) 563–575.
- [13] S.J. Mulligan, B.A. MacVicar, Calcium transients in astrocyte endfeet cause cerebrovascular constrictions, *Nature* 431 (2004) 195.
- [14] V. Parpura, P.G. Haydon, Physiological astrocytic calcium levels stimulate glutamate release to modulate adjacent neurons, *Proc. Natl. Acad. Sci. U.S.A.* 97 (15) (2000) 8629–8634.
- [15] C. Gwizdala, C.V. Singh, T.R. Friss, J.C. MacDonald, S.C. Burdette, Quantifying factors that influence metal ion release in photocaged complexes using ZinCast derivatives, *Dalton Trans.* 41 (26) (2012) 8162–8174.
- [16] K. Barbeau, E.L. Rue, K.W. Bruland, A. Butler, Photochemical cycling of iron in the surface ocean mediated by microbial iron(III)-binding ligands, *Nature* 413 (6854) (2001) 409–413.
- [17] F.C. Küpper, C.J. Carrano, J.-U. Kuhn, A. Butler, Photoreactivity of iron (III)-aerobactin: photoproduct structure and iron(III) coordination, *Inorg. Chem.* 45 (15) (2006) 6028–6033.
- [18] H. Sayre, K. Milos, M.J. Goldcamp, C.A. Schroll, J.A. Krause, M.J. Baldwin, Mixed-donor, α-hydroxy acid-containing chelates for binding and light-triggered release of iron, *Inorg. Chem.* 49 (10) (2010) 4433–4439.
- [19] L. Brülisauer, M.A. Gauthier, J.-C. Leroux, Disulfide-containing parenteral delivery systems and their redox-biological fate, *J. Controlled Release* 195 (Supplement C) (2014) 147–154.
- [20] M.H. Lee, Z. Yang, C.W. Lim, Y.H. Lee, S. Dongbang, C. Kang, J.S. Kim, Disulfide-cleavage-triggered chemosensors and their biological applications, *Chem. Rev.* 113 (7) (2013) 5071–5109.
- [21] S. Moosun, S.J. Lallou, M.G. Bhowon, Metal complexes of diaryl and 2,2'-dipyridyl disulfides, *J. Sulfur Chem.* 33 (6) (2012) 661–691.
- [22] P.E. Riley, K. Seff, Crystal and molecular structure of chloro[bis(2-[(2-pyridylmethyl)amino]ethyl) disulfide]nickel(II) perchlorate, *Inorg. Chem.* 11 (12) (1972) 2993–2999.
- [23] M.M. Kadooka, L.G. Warner, K. Seff, Crystal and molecular structure of dichloro[bis(2-pyridyl) disulfide]cobalt(II), *Inorg. Chem.* 15 (4) (1976) 812–816.
- [24] J.A. Bertrand, J.L. Breece, Preparation and structure of chloro[bis(salicylideneimine-phenyl)disulfide]iron(III), *Inorg. Chim. Acta* 8 (1974) 267–272.
- [25] A. Elmali, Y. Elerman, Crystal structure of chloro[bis(5-bromo-salicylideneimine-phenyl)disulfide]-iron(III) complex, *Anal. Sci.* 18 (12) (2002) 1399–1400.
- [26] M.G. Bhowon, S. Jhaumeer-Lallou, N. Soukhee, A. Allibacus, V. Shiboo, Synthesis, catalytic and antibacterial activity of 2-aminophenyldisulphide, *J. Coord. Chem.* 60 (12) (2007) 1335–1343.
- [27] R. Roy, S. Sproules, T. Weyhermüller, K. Wieghardt, Trivalent iron and ruthenium complexes with a redox noninnocent (2-mercaptophenylimino)-methyl-4,6-di-tert-butylphenolate(2-) ligand, *Inorg. Chem.* 48 (8) (2009) 3783–3791.
- [28] A. Donzelli, I. Metushi, P.G. Potvin, Titanium(IV) complexes of disulfide-linked schiff bases, *Inorg. Chem.* 51 (9) (2012) 5138–5145.
- [29] G. Prakash, R. Ramachandran, M. Nirmala, P. Viswanathamurthi, W. Linert, Catalytic role of ruthenium(III) complexes bearing cystamine-based disulfide ligands on the N-alkylation of o-substituted anilines, *Monatsh. Chem.* 145 (12) (2014) 1903–1912.
- [30] R. Uma, M. Palaniandavar, Copper(II)-disulphide interaction in copper complexes containing salicylaldehyde and pyridylaldehyde ligands: synthesis, spectra and redox behaviour, *Trans. Met. Chem.* 18 (6) (1993) 629–634.
- [31] H.F. Hsu, C.L. Su, N.O. Gopal, C.C. Wu, W.C. Chu, Y.F. Tsai, Y.H. Chang, Y.H. Liu, T.S. Kuo, S.C. Ke, Redox chemistry in the reaction of oxovanadium(V) with thiolate-containing ligands: the isolation and characterization of non-oxo vanadium(IV) complexes containing disulfide and thioether groups, *Eur. J. Inorg. Chem.* 2006 (6) (2006) 1161–1167.
- [32] J.W. Pyrz, X. Pan, D. Britton, L. Que, Models for catechol dioxygenases. Structure of bromobis[2-(2'-hydroxyphenyl)benzothiazolato]iron(III) derived from the bromoiron(III) complex of 2,2'-bis(salicylideneamino)phenyl) disulfide, *Inorg. Chem.* 30 (18) (1991) 3461–3464.
- [33] T.M. Chang, E. Tomat, Disulfide/thiol switches in thiosemicarbazone ligands for redox-directed iron chelation, *Dalton Trans.* 42 (22) (2013) 7846–7849.
- [34] M.Y. Hamed, J. Silver, M.T. Wilson, Studies of the reactions of ferric iron with glutathione and some related thiols, *Inorg. Chim. Acta* 78 (1983) 1–11.
- [35] K.A. Johnson, Z.B. Simpson, T. Blom, Global kinetic explorer: a new computer program for dynamic simulation and fitting of kinetic data, *Anal. Biochem.* 387 (1) (2009) 20–29.
- [36] G. Louit, S. Foley, J. Cabillic, H. Coffigny, F. Taran, A. Valleix, J.P. Renault, S. Pin, The reaction of coumarin with the OH radical revisited: hydroxylation product analysis determined by fluorescence and chromatography, *Radiat. Phys. Chem.* 72 (2) (2005) 119–124.
- [37] Z.-R. Lin, L. Zhao, Y.-H. Dong, Quantitative characterization of hydroxyl radical generation in a goethite-catalyzed Fenton-like reaction, *Chemosphere* 141 (2015) 7–12.
- [38] C.B.C. Rutely, F. Jean-M, Z.T. Walter, D.-B. Xochitl, S. Mika, Towards reliable quantification of hydroxyl radicals in the Fenton reaction using chemical probes, *RSC Adv.* 8 (10) (2018) 5321–5330.